Exploration of Neuroprotective Therapy

Open Exploration

Open Access Original Article

Passive immunization against amyloid peptide restores pattern separation deficits in early stage of amyloid pathology but not in normal aging

Karin Herbeaux[1], Christopher Borcuk[1], Caroline Mursch[1], Véronique Kemmel[2], Olivier Bousiges[1,2], Anne-Laurence Boutillier[1], Chantal Mathis[1†], Céline Héraud[1†*]

[1]Laboratoire de Neurosciences Cognitives et Adaptatives, CNRS UMR 7364, University of Strasbourg, 67000 Strasbourg, France

[2]Laboratory of Biochemistry and Molecular Biology, University Hospital of Strasbourg, Avenue Molière, Hôpital de Hautepierre, 67000 Strasbourg, France

[†]These authors contributed equally to this work.

***Correspondence:** Céline Héraud, Laboratoire de Neurosciences Cognitives et Adaptatives, CNRS UMR 7364, University of Strasbourg, 12 rue Goethe, 67000 Strasbourg, France. cheraud@unistra.fr

Academic Editor: Rodrigo Pacheco, Universidad San Sebastián, Chile

Received: February 9, 2025 **Accepted:** May 6, 2025 **Published:** June 16, 2025

Cite this article: Herbeaux K, Borcuk C, Mursch C, Kemmel V, Bousiges O, Boutillier AL, et al. Passive immunization against amyloid peptide restores pattern separation deficits in early stage of amyloid pathology but not in normal aging. Explor Neuroprot Ther. 2025;5:1004108. https://doi.org/10.37349/ent.2025.1004108

Abstract

Aim: Aging and early Alzheimer's disease (AD) affect pattern separation (PS) based mnemonic discrimination in humans. PS function involves the dentate gyrus (DG), a brain region producing new neurons during adulthood. Aging and AD presumably affect PS and DG function through different mechanisms, although it has never been clearly shown within the same study. Passive immunotherapy targeting β-amyloid peptides (Aβ) was used to determine the relative contribution of abnormal levels of Aβ to early PS deficits in two mouse models of aging and amyloid pathology, and potential involvement of adult neurogenesis.

Methods: Female Tg2576 mice were tested in a spatial PS task from the age of three months to determine the age of onset of PS deficits. A cohort of five-month-old female Tg2576 mice and a cohort of 20-month-old male C57BL/6J mice were treated with passive immunization for four weeks, and then tested for PS performance. ELISA assays were used to quantify Aβ levels in CA3/DG regions of these mouse models. DG recruitment during PS testing was assessed with an Egr-1 ex vivo imagery. The contribution of adult-born neurons to a potential rescue of PS performances was evaluated using bromodeoxyuridine and doublecortin co-immunostainings.

Results: Spatial PS deficits appeared first in four-month-old female Tg2576 mice, an early pre-plaque stage of Alzheimer pathology. Aβ immunotherapy restored PS performance in Tg2576 mice, but not in aged male C57BL/6J mice. PS impairments were associated with an overactivation of the DG in both models and a potentially abnormal level of immature adult-born neurons in Tg2576 mice.

Conclusions: Alleviation of PS deficits following Aβ immunotherapy in Tg2576 mice is associated with reduced DG activation and improved adult-born neurons maturation. The absence of beneficial effects in aged mice suggests that PS deficits in aging and AD may be related to different underlying mechanisms.

Keywords

Aβ passive immunotherapy, Alzheimer's disease, aging, pattern separation, dentate gyrus, knock-in mouse model

Introduction

Alzheimer's disease (AD) is the most common neurodegenerative disease affecting the elderly. In the majority of cases, people who develop the disease are aged 65 or older (late-onset) while in a small number of cases, AD appears before the age of 65 (early-onset) due to genetic mutations. One of the earliest signs of AD is an increase in β-amyloid peptide (Aβ) levels in the brain, which can be detected 15 to 20 years before diagnosis [1–3]. This finding has prompted extensive research focusing on preclinical stages to improve our understanding of initial events leading to the disease. Although the priority is to find early therapeutic targets, it is crucial to identify early biomarkers. Identification of AD in patients before the onset of clinical symptoms would enable early diagnosis, prevention, and proactive treatment. Special efforts have been made to develop new behavioral assays capable of detecting early cognitive dysfunctions in people at risk for developing AD [4–6]. Among these assays, behavioral pattern separation (PS) evaluates the ability of individuals to disambiguate between memories of similar events, a paradigm based on a model of hippocampal computation [7–9]. There is evidence that PS tasks may be useful in detecting subpopulations at risk of developing mild cognitive impairment (MCI). Spatial PS tasks based on object displacements further allowed to discriminate two subpopulations within elderly adults, those with healthy aging (unimpaired in neuropsychological tests sensitive to early stages of AD) and those with pathological aging (impaired in these neuropsychological tests) [10, 11]. In brain imaging studies, PS performance of the cognitively normal elderly showed an inverse correlation with test-induced functional magnetic resonance imaging BOLD activation within the Ammon's horn 3/dentate gyrus (CA3/DG) region, and a positive correlation with perforant path integrity [8, 12]. Thus, PS deficits may reflect altered ability of the DG to orthogonalize perforant path inputs originating from entorhinal layer II, which is one of the very first regions showing neuronal loss in AD.

Animal research provided evidence supporting the role of the dorsal DG in PS using lesioned rats tested in spatial separation paradigms [13, 14]. This role was further confirmed with electrophysiological recordings in rats [15–17], and genetic manipulations leading to DG dysfunctions in mice [18–20]. Adult neurogenesis in the dorsal DG was proposed to play a key role in the ability to discriminate similar memories [21–23]. Indeed, ablation or silencing of adult-born DG neurons through pharmacological treatment or genetic manipulation resulted in PS deficits, whereas alternative strategies designed to increase the survival of new neurons were shown to improve PS performance [21–24]. Many studies showed that PS performance is impaired in aged rodents using object and spatial separation paradigms [25–27]. Alternatively, some studies suggested the role of a substantial age-dependent reduction in neurogenesis in PS deficits in old C57BL/6J mice (B6 mice) [28, 29]. PS deficits were also shown in mouse models of AD [30–33]. In summary, although aging and the early stages of AD are based on different neuropathological processes, both display PS deficits, which appear related to altered function in the DG. Whether these functional alterations could rely on the same neurobiological substrates remains to be determined.

In the present study, we first determined the age of onset of PS deficits in the Tg2576 (Tg) mouse model of AD, characterized by a slow progression of amyloid pathology [34]. The tests were performed in a spatial PS paradigm based on the detection of discrete changes in object location, which has been previously used to show PS deficits in aged B6 mice [29]. As PS deficits appeared in young Tg at an early

preplaque stage, they provided an ideal model to test if early decrease in Aβ levels could improve PS performance using passive immunization treatment with m266, a monoclonal antibody neutralizing Aβ species [35]. In parallel, the effect of passive immunization was also evaluated on PS deficits in 20-month-old B6 mice to verify whether aged-dependent murine Aβ accumulation could also contribute to these deficits. Interestingly, m266 immunotherapy efficiently restored PS abilities in young Tg but not in aged B6 mice. We then evaluated the effect of m266 treatment on neuronal activity by ex vivo imagery of the immediate early gene *Zif268*/*Egr-1* (*egr1*, early growth response 1) [36]. We specifically chose Egr-1 due to its high expression in hippocampus and its role in the selection and maturation of DG newborn neurons [37]. We also quantified the involvement of adult neurogenesis in the beneficial effects of the m266 treatment, especially observed in young Tg mice. Finally, background levels of Aβ species were determined in the CA3/DG region by ELISA assays for each model.

Materials and methods

Animals

All procedures were performed in accordance with European Directives (2010/63UE) and were approved by a local ethical committee (Comité Régional d'Ethique en Matière d'Expérimentation Animale de Strasbourg CEEA 35, reference # 02965.02). The APPSWE (Tg) mouse line carries a transgene coding for the 695-amino acid human amyloid precursor protein (APP) isoform containing the double Swedish mutation (K670N, M671L) [34] which leads to high brain concentrations of Aβ and significant amyloid deposition around the age of 8 months. Female Tg and non-transgenic (NTg) littermates (model 1349-RD1-F, Taconic Bioscience, Germantown, USA) were Rd1 tested to ensure these subjects were not homozygous for the *Pde6b*^{rd1} mutation (i.e., not blind). Thirteen female Tg and NTg mice were assigned to the experiment aiming to define the earliest age of deficits in the PS task. Thirty-five Tg [24 tested and 11 home cage (HC)] and 15 NTg (10 tested and 5 HC) female mice were assigned to the Tg mice anti-Aβ antibody study. Forty-nine male C57BL/6J (B6) mice were used in the aged mice anti-Aβ antibody study: 35 mice were 20-month-old (24 tested and 11 HC) and 14 mice were five-month-old mice (10 tested and 4 HC). Upon arrival, mice were group-housed in standard cages with food and water available ad libitum. Nesting material and a few food pellets were added to the bedding to favor natural behavior expression. A plastic tunnel (4 cm in diameter, 15 cm long) was provided one week before behavioral testing. Two days prior to behavioral testing, mice were familiarized with tube transportation from their HC to their holding cage and vice versa. The same tube was used for all transports between HC, holding cage, and testing apparatus [38]. The housing room was kept at a controlled temperature (23°C ± 1°C) with a 12/12-hour light/dark cycle (lights on at 8.00 AM). Behavioral testing took place between 9.00 AM and 4.00 PM. General health status was checked before the beginning of the experiments and animals lacking vibrissae (barbering) or showing eye abnormalities (e.g., cataract or closed eye) were not tested.

Behavioral PS task

The PS task is based on the spontaneous tendency of mice to explore an object displaced in a familiar context [39]. It resembles the classical object location test except that in our PS test, the object displacement was set at 20 cm, the distance detected by six-month-old B6 mice but not 20-month-old mice, as described in Cès et al. [29]. A longer 35-cm displacement test was integrated into the task as a control for the preserved ability to detect large object displacement. Briefly, mice were first familiarized with the large, dimly lit open field (92.5 cm × 92.5 cm × 35 cm; Ugo Basile, Italy; ~11 lux in the center) for 8–10 min. During the next three days, they underwent a daily two-trial session: i) habituation with no object displacement, ii) testing with long-distance 35 cm displacement, and iii) testing with the critical 20 cm object displacement, with each day involving a different set of objects (see Figure 1A). During each session, mice could explore the two objects located 20 cm apart diagonally in the open field during the acquisition trial. The sessions lasted for 12 min in studies using young Tg and NTg female mice and 15 min in the study using old B6 male mice, as aged mice often explore less than young mice [29]. After a 5-min intermission in their holding cage, mice returned to the open field for a 6-min retention trial with one of the two objects

diagonally moved 0, 35, or 20 cm away from the fixed object. Object exploration was only considered when mice engaged in active exploration i.e., when the nose was within two cm facing the object. Discrimination performance was evaluated as the percentage of time spent exploring the displaced object relative to the total time spent exploring the two objects during the first three minutes of the test trial, as the mice tended to ignore the objects during the remaining three minutes. All objects were made of glass or plastic (5–6.5 cm diameter and 4.5–7 cm high). Data from one vehicle-treated aged mouse was excluded due to exaggerated thigmotaxis behavior, which biased performance (0 cm: 0%; 35 cm: 56.9%; 20 cm: 27.1%).

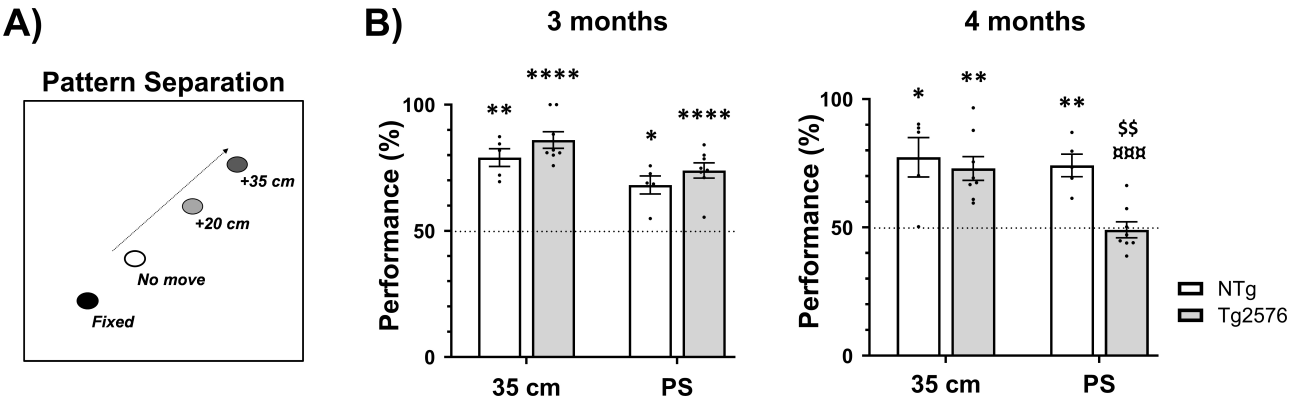

Figure 1. Spatial PS deficits first appeared in 4-month-old Tg2576 mice. (**A**) Experimental procedure for spatial PS task. First, mice carried out a habituation with no object displacement. The next day, mice were tested with 35-cm object displacement and the last day, with 20-cm object displacement. (**B**) PS performance was altered only in 4-month-old Tg2576 mice whereas 35-cm object displacement was detected at both ages in both genotypes. Data were analyzed by a two-way ANOVA followed by Tukey's multiple comparisons post hoc test: $^{\$\$}$ $P < 0.01$ versus other groups for PS; $^{¤¤¤}$ $P < 0.001$, versus 35-cm performance for the same group. A student's *t* test was carried out for each group compared to the 50% chance level (dot lines): * $P < 0.05$, ** $P < 0.01$, and **** $P < 0.0001$. PS: pattern separation

Anti-Aβ antibody and BrdU treatments

Aβ passive immunization was performed with the m266 antibody (gift from Boehringer Ingelheim, Biberach an der Riss, Germany). The m266 stock solution was at a concentration of 2.2 mg/mL in 20 mM sodium acetate (Sigma-Aldrich), 140 mM sodium chloride (Fisher Chemical, Denmark), and 0.02% Tween 80 (pH 5.5) (P1754, Sigma-Aldrich). Female Tg and NTg mice and male B6 mice received a five mg/kg (0.1 mg/mL, 10 mL/kg) intraperitoneal (IP) injection of m266 or its vehicle (20 mM sodium acetate, 140 mM sodium chloride, and 0.02% Tween 80) once a week during four weeks at 4.30 PM (see Figure 1A). This protocol was adapted from a study on PDAPP mice, an amyloid mouse model [40]. The last injection was given on the day of familiarization to the open-field, three days before PS testing. The day after the first m266 injection, all mice received an IP injection of 5-bromo-2-deoxyuridine [BrdU; B5002, Sigma-Aldrich, Hamburg, Germany; diluted in 0.1 M phosphate buffer (0.081 M Na_2HPO_4, 0.018 M NaH_2PO_4)] (Carl Roth, Karlsruhe, Germany), pH 8.4, 40°C, 100 mg/kg/injection, 0.1 mL/kg/injection twice a day (8.30 AM, 4.30 PM) for four days. The last BrdU injection was made 28 days before testing PS performance.

Brain fixation and immunochemistry

Ninety minutes after the PS test completion, brains were processed for immunohistochemistry. We collected brains from five NTg, five vehicle-, and six m266-treated Tg female mice, as well as four young male B6 mice, five vehicle-, and six m266-treated aged male B6 mice from the tested groups. For control groups [mice which remained in their home cage (HC groups) during the whole process as controls for the tested groups], we collected brains from five NTg, four vehicle-, and six m266-treated Tg female mice, four young male B6 mice, six vehicle-, and five m266-treated aged male B6 mice. Under deep anesthesia [120 mg/kg pentobarbital (Ceva Santé Animale, Libourne, France), 10 mL/kg, IP], an intracardiac perfusion with phosphate-buffered saline (PBS) [0.01 M PBS, 0.1% heparin (Héparine Choay, CheplaPharm, Arzneimittel GmbH, GR, Germany)] was carried out, followed injection of a fixative solution [4% paraformaldehyde (Carl Roth GmbH + Co KG, Germany) in 0.1 M phosphate buffer, pH 7.4, 4°C]. Brains were postfixed for 24 h in 4% paraformaldehyde and stored in PBS all at 4°C. Fifty µm-thick coronal sections were obtained with a

vibratome (Leica Biosystems) and were stored free-floating at –20°C in a cryostorage solution [30% glycerol, 30% ethylene glycol (both from Carl Roth GmbH, Karlsruhe, Germany), 0.026 M phosphate buffer].

NTg and Tg brain sections were PBS-rinsed, and then incubated for 15 min in 2 N hydrochloric acid (Carl Roth GmBH) at 37°C. After washing, they were blocked in 5% normal goat serum in PBS with 0.5% Triton X100 (T9284, Sigma-Aldrich), followed by a 48 hour-incubation at room temperature in a solution combining three antibodies: monoclonal rat anti-BrdU antibody (1/500, ab6326, Abcam) with polyclonal rabbit anti-Egr-1 (1/300, 4153S, Cell signaling, Massachusetts, USA), and polyclonal guinea pig anti-doublecortin (DCX) antibodies (1/5,000, ab2253, Millipore, Temecula, CA, USA). After several washes, sections were incubated in secondary antibody solution: goat anti-rat Alexa 555 with goat anti-mouse Alexa 647 and goat anti-rabbit Alexa 488, or with goat anti-guinea pig Alexa 488 and goat anti-rabbit Alexa 647 (for all: 1/500, Life Technologies, Eugene, OR, USA) 2 h at room temperature. After final washing, sections were mounted in Fluoromount (F4680, Sigma-Aldrich) and stored at 4°C.

BrdU, a thymidine analog incorporated in DNA into dividing cells can be used for birth dating. DCX is commonly recognized as a marker of adult-born neuronal cells within the DG [41–44] allowing the identification of new neuronal progenitors (around 8–15 days post-birth) and new immature neurons (around 15–30 days post-birth) [45, 46]. Thus, in our study, co-labeling of $BrdU^+/DCX^+$ was used to identify immature neurons. *Egr-1* is an immediate early gene whose expression is associated with neuronal activity as already shown in adult-born and pre-existing granular cells of the DG [42, 47–52].

Immunohistochemistry for aged mice was carried out with a colorimetric protocol to avoid age-dependent autofluorescence (age-dependent accumulation of lipofuscins). Thus, for Egr-1 staining, brain sections were PBS-rinsed and then incubated for 15 min in 2 N hydrochloric acid (Carl Roth GmbH, Karlsruhe, Germany) at 37°C followed by washing. After washing, sections were incubated in 0.3% hydrogen peroxide (216763, Sigma-Aldrich) in methanol for 30 min at room temperature to quench endogenous peroxidase activity, rinsed several times, blocked in 5% normal goat serum in PBS-0.5% Triton X100 and then incubated in the polyclonal rabbit anti-Egr1 (1/1,000, 4153S, Cell signaling) during 48 h at room temperature. After several washes, sections were incubated with biotinylated goat anti-rabbit antibody (1/500, Vector Laboratories, Burlingame, California) for two hours at room temperature followed by a 45 min incubation with avidin-biotin-peroxidase complex (Vectastain ABC kit; Vector Laboratories, Burlingame, California, USA). Staining was developed at room temperature with 3,3'-diaminobenzindine (DAB kit, Vector Laboratories, Burlingame, California, USA), and the reaction was stopped by rinses in PBS.

Quantification of positively labeled cells

Triple immunostainings were analyzed with the Leica Application Suite X Office (Leica microsystems) using confocal images obtained with a Leica TCS SP5 II. Cell counting was carried out in the granule cell layer (GCL), including the subgranular zone (two-cell-thick region along the inner GCL border) of the dorsal DG (called after in the paper just "GCL"), in every fifth section (50 µm thick, 250 µm apart) spanning between –0.94 mm (first section) to –2.06 mm from the bregma. Counting was performed through the entire slice in five sections per mouse. Only well-defined and round/ovoid nuclei were counted. These are indeed more likely to correspond to new GCs since new glial cells migrate mainly into the hilum and rarely into the GCL [53]. The experimenter was blind to both the genotype and treatment. The GCL area was measured for each section with ImageJ software (National Institute of Health, Bethesda, MD), on DG images captured with the 4× objective of an Olympus AHBT3 microscope [54]. GCL volume for each section was obtained by multiplying the total GCL area (left GCL + right GCL) by the section thickness. For each mouse, the density of BrdU or Egr-1 positive cells ($BrdU^+$ or $Egr\text{-}1^+$) was calculated by dividing the total counts of $BrdU^+$ or $Egr\text{-}1^+$ cells by the total volume of GCL screened. The total number of $BrdU^+$ cells was calculated by multiplying the density by the GCL reference volume. This reference volume was determined by multiplying the GCL area by the distance between sampled sections (250 µm). The percentage of cells expressing the immature neuron maker (DCX) among the four-week-old $BrdU^+$ cell population was calculated as: 100× number of double stained cells/total number of $BrdU^+$ cells. The percentage of triple stained cells ($BrdU^+/DCX^+/Egr\text{-}1^+$) was calculated as: 100× number of triple stained cells/total number of $BrdU^+/DCX^+$ neurons.

For Egr-1 staining of B6 sections, digital images of the DG in both hemispheres were captured using a Hamamatsu NanoZoomer S60 Digital slide scanner. Five consecutive coronal sections (each 250 µm apart) were taken from each mouse. The GCL of the DG was delimitated based on the 3rd edition brain atlas of Franklin and Paxinos [55]. The images of the delimitated GCL were converted into 8-bit greyscale and immunopositive cells were counted using ImageJ. Egr-1 positive cells were defined as having immunopositive nuclei (diameter of 4–20 µm, sphericity of above 0.1) stained below a grayscale threshold set directly below the background peak visualized by a pixel intensity histogram. The greyscale threshold was set manually by an experimenter who remained blind to group conditions. Cell density was defined as the total number of Egr-1 positive nuclei divided by the total volume/area across all sections of the GCL.

ELISA dosage

After cervical dislocation, hippocampal regions from four vehicle- and six m266-treated Tg mice, five young B6 mice, four vehicle and six m266-treated aged B6 mice were quickly removed, frozen in liquid nitrogen, and stored at –80°C. Aβ quantification was performed on the CA3/DG region, as its dentate adult-born neurons are thought to be involved in PS function. Samples were homogenized in 10 volumes of ice-cold guanidine buffer (5 M guanidine-HCl/50 mM Tris–Cl, pH 8.0, G3272 and T3253 respectively, Sigma-Aldrich), mixed for three hours at room temperature and diluted to 1:10 in PBS containing 1% BSA, 0.05% Tween20 (from the ELISA kit) supplemented with protease inhibitor cocktail (P8340, Sigma-Aldrich), phosphatase inhibitor cocktail (PhosStop, 4906845001, Roche Diagnostics GmbH, Mannheim, Germany), and 1 mM phenylmethylsulfonyl fluoride (Sigma-Aldrich). The CA3/DG homogenates were centrifuged at 16,000 *g* for 20 minutes at 4°C and supernatants were aliquoted. Protein concentration was measured using the Bio-Rad Protein Assay (5000006, Bio-Rad Laboratories, CA, USA). Total levels of human Aβ40 and Aβ42 were determined using the human Aβ(1–40) and Aβ(1–42) high sensitivity ELISA kits (RE59781 and RE59791, respectively) whereas total levels of murine Aβ40 and Aβ42 were determined by using the amyloid-beta (1–40) (Mouse/Rat) and the amyloid-beta (1–42) (Mouse/Rat) ELISA kits (RE45741 and RE45721, respectively). All kits were purchased IBL International (Hambourg, Germany) and used following the manufacturer's instructions. The signal was normalized to the protein concentration for each sample. All dosages were done in duplicate, and samples with > 10% variation between duplicates were discarded from analysis.

Statistical analysis

Statistical analysis was completed using GraphPad Prism 7 (GraphPad Inc) and Statistica 13.3 (TIBCO Software Inc). For behavioral data, the main effects were tested with a two-way ANOVA with repeated measures (group × distance). For each distance, groups were compared with a one-way ANOVA when relevant (group). ANOVAs were followed by the post hoc Tukey's multiple comparisons test (Tukey). In addition, the performance level for each group was compared to the 50% chance level using student's *t* test. For immunohistochemical experiments, data sets were analyzed using the non-parametric Kruskal-Wallis (KW), Mann-Whitney (MW), and Wilcoxon (W) tests, as group sizes were relatively small. The Wilcoxon signed rank test (WSR) was used to compare upper and lower blade data. Two-way ANOVAs, with repeated measures when relevant (lower and upper blades), were also performed to test possible interactions (groups, HC, and tested conditions). Whenever outcomes were complementary or differed from non-parametric tests, parametric statistics were reported in the result section. The MW was used for ELISA data. Outliers were identified with the ROUT method in GraphPad prism. Differences were considered significant at $P < 0.05$. All data are given as mean ± standard error of the mean (SEM) including data analyzed with non-parametric tests instead of median and inter-quartile range.

Results

Early PS deficits in Tg mice

The behavioral task measures the ability of the mice to detect the move of one of two similar objects. For this experiment, we used the 35-cm displacement as the easy distance and the 20-cm displacement as the

difficult/PS distance (Figure 1A). From the age of three months, eight Tg mice and five NTg female mice were tested every month to find the age of onset of PS deficits. At the age of three months, both Tg mice and NTg mice performed above chance level on the easy 35-cm test and the difficult/PS 20-cm test (Figure 1B). When retested at the age of four months, Tg mice were selectively impaired in the detection of the difficult/PS 20-cm displacement while NTg mice maintained high performance on both 20-cm and 35-cm tests (group: $F1,11 = 6.95$, $P = 0.02$; test: $F1,11 = 10.4$, $P = 0.008$; group × test: $F1,11 = 6.1$, $P = 0.03$; Figure 1B). We verified that the two groups similarly explored objects during acquisition trials (Figure S1). Taken together, these results indicate that a specific deficit in the spatial PS test appeared in 4-month-old Tg mice.

Effect of m266 on PS performance in Tg2576 mice

We then tested the effect of an immunotherapy treatment using m266 anti-Aβ antibody on PS performance. Four-month-old Tg female mice ($n = 12$) were treated with m266 (5 mg/kg body weight) or vehicle ($n = 12$) once per week for four weeks with the last injection given on the day of familiarization to the open field (Figure 2A). Due to an object handling error in the PS test, we discarded one vehicle-treated mouse (final $n = 11$). Vehicle-treated NTg mice ($n = 10$) were used as an internal control for the validity of the PS test (20 cm displacement). The performances of the different groups differed depending on the distance tested (group: $F2,30 = 9.1$, $P = 0.0008$; test: $F1,30 = 15.6$, $P = 0.0004$; group × test: $F2,30 = 13$, $P < 0.0001$; Figure 2B). All groups performed similarly and above chance level in the 35-cm test. As expected, PS performance of five-month-old vehicle-treated Tg mice did not differ from chance level, as found in four-month-old Tg. However, m266 treatment was able to statistically prevent this early deficit in Tg mice ($F2,30 = 19.1$, $P < 0.0001$) which performed as well as vehicle-treated control NTg mice (Figure 2B). Of note, both Tg groups explored the objects less than NTg mice; m266 did not improve this genotype effect on exploration behavior (group: $F2,30 = 7.6$, $P = 0.002$; test: $F1,30 = 8.1$, $P = 0.008$; group × test: $F2,30 = 0.4$, $P = 0.7$; Figure S2A), suggesting the treatment had no effect on object exploration behavior during this task.

Effect of m266 on PS performance in aged B6 mice

We next tested whether m266 treatment could reverse PS deficits previously described in aged B6 male mice [29]. B6 males were treated with m266 (5 mg/kg body weight, $n = 12$) or vehicle ($n = 12$) once per week during four weeks with the last injection administered the first day of behavioral testing (Figure 2A) at 20 months of age (Figure 2C). Young vehicle-treated B6 males ($n = 10$) served as internal controls to validate the PS test at the age of 4 months. Group performances differed as a function of the distance tested (group: $F2,30 = 10.6$, $P = 0.0003$; test: $F1,30 = 49.8$, $P < 0.0001$; group × test: $F2,30 = 4.6$, $P = 0.02$; Figure 2C). The young mice group outperformed both aged groups in the PS test. Notably, aged vehicle- and m266-treated groups showed similar PS deficits with performance at chance level: chronic m266 treatment did not prevent PS deficits in aged B6 mice. Both aged groups succeeded in detecting the 35-cm object displacement. During the acquisition trials, all groups spent similar time exploring the two objects (group: $F2,30 = 0.4$, $P = 0.7$; test: $F1,30 = 1.8$, $P = 0.2$; group × test: $F2,30 = 0.3$, $P = 0.7$; Figure S2B). Thus, in aged mice, m266 treatment had no effect on initial exploration of the objects and retention performances in both the 35-cm and the PS tests.

Impact of early amyloidopathy on Egr-1 activation in the GCL of PS tested mice

The GCL of the dorsal DG is considered part of the neuronal circuit involved in PS. To understand whether PS deficits in Tg and aged mice could result from impaired neuronal activation during the test, we investigated Egr-1 immunostaining in the dorsal GCL. Increase of Egr-1 expression in adult-born and pre-existing granular cells of the DG was already shown after behavioral tasks [47–49, 51]. We also tested whether PS deficiency is associated with impaired adult neurogenesis by staining newly formed neurons with anti-DCX and anti-BrdU antibodies. Thus, triple BrdU/DCX/Egr-1 immunostainings were carried out in young NTg and Tg female mice (Figure 3A). Due to the extremely low levels of newborn neuronal cells in the GCL of aged B6 male mice [29], we only carried out Egr-1 immunostaining in this group and its young counterpart. These immunostainings were performed on brains collected 90 min after completion of the PS

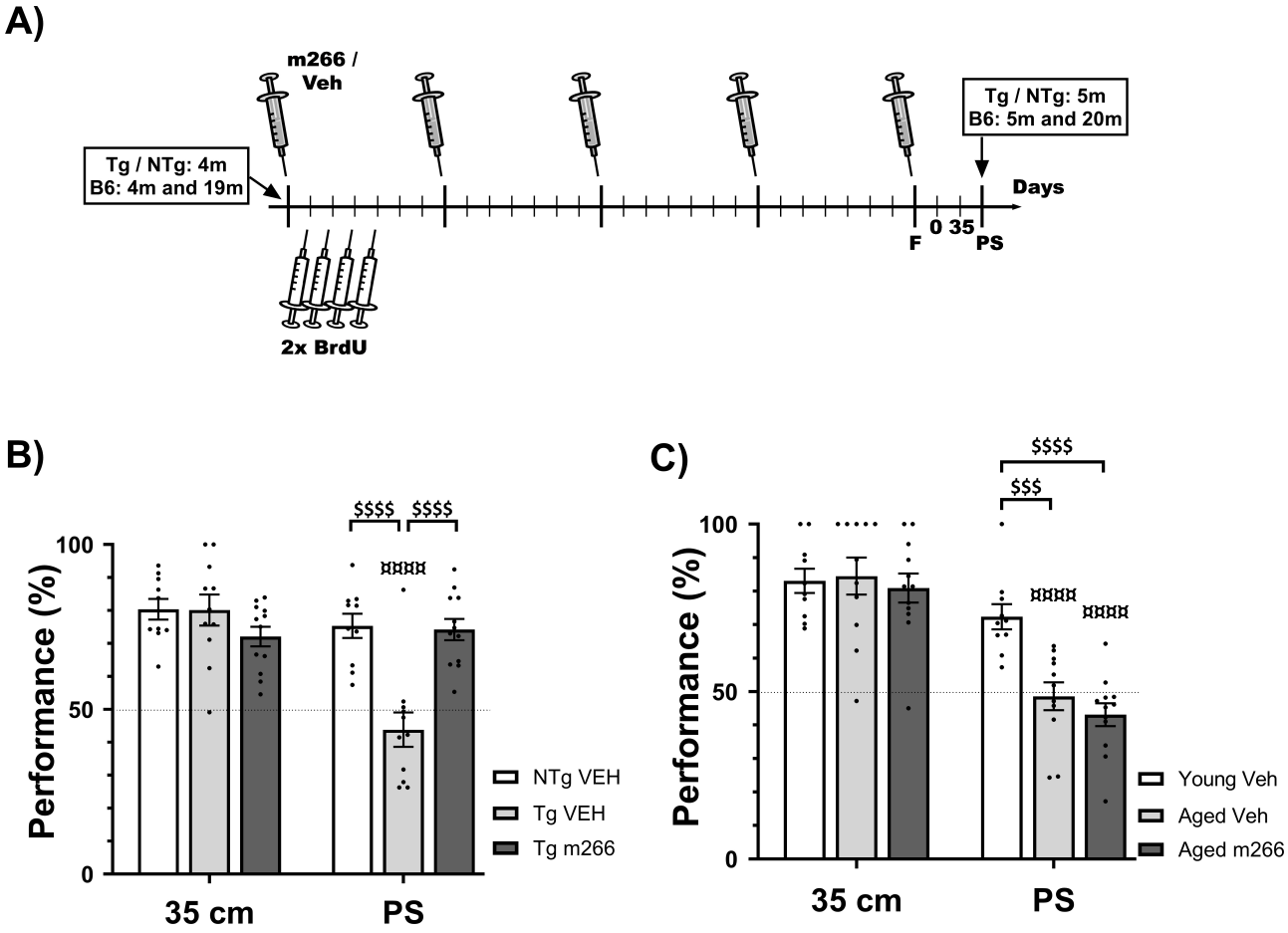

Figure 2. Chronic m266 treatment rescued PS performance in Tg2576 mice but not in aged C57BL/6J mice. (**A**) Injection schedule for m266 or vehicle (veh) once per week, BrdU twice a day during four days on the first week, the last four days were devoted to open-field familiarization (F), 0-cm, 35-cm and PS 20-cm displacement tests. m: months. (**B**) PS deficits in 5-month-old Tg mice was prevented by chronic m266 treatment. (**C**) PS deficits in 20-month-old B6 mice were not prevented by chronic m266 treatment. Data are expressed as mean (± SEM) of the percent of time spent exploring the displaced object relative to the total time spent exploring the two objects. Tukey's multiple comparisons test: $^{\$\$\$}$ $P < 0.001$, $^{\$\$\$\$}$ $P < 0.0001$ versus other groups for PS; $^{¤¤¤¤}$ $P < 0.0001$ versus 35-cm performance. Dot line: 50% chance level; PS: pattern separation

test, to allow Egr-1 protein expression, in a subset of NTg, Tg, and B6 groups treated with vehicle or m266, and a subset of NTg, Tg, and B6 groups also treated with m266 or vehicle but left in their HC (non-tested).

In the Tg mice experiment, the density of Egr-1$^+$ cells in the GCL was increased about 2-fold in the tested mice (mean = 29.7 ± 3.6 cells/0.001 mm^3) compared to the HC mice (mean = 14.2 ± 1.3 cells/0.001 mm^3; MW: $U = 18$, $Z = -3.9$, $P < 0.0001$; one m266-treated Tg was excluded as an outlier, Figure 3B and Table S1), showing that neuronal activity has indeed increased in the GCL of mice tested for PS. However, the level of GCL activation clearly differed among the three tested groups (KW: $H = 6.3$, $P = 0.04$) with m266-treated Tg mice showing lower levels than vehicle-treated Tg mice (MW: $U = 1$, $Z = 2.4$, $P = 0.02$). The level of activation remained stable among HC groups (KW: $H = 0.6$, $P = 0.7$). Thus, a global activation of the GCL was induced by the behavioral task compared to HC controls and this activation was lower in m266-treated Tg mice.

When the upper and lower blade of the DG were quantified separately, we found that the upper blade was globally more active than the lower blade (pooled mice WSR: $Z = -4.3$, $P < 0.0001$, Figure 3C, Table S1). This effect was even more pronounced in tested mice than in HC mice (pooled tested mice: upper = 42.2 ± 3.5 versus lower = 22.1 ± 1.7 cells/0.001 mm^3, WSR: $Z = 3.4$, $P = 0.0007$; pooled HC groups: upper = 17.7 ± 2.8 versus lower = 13.0 ± 1.7 cells/0.001 mm^3, WSR: $Z = 2.2$, $P = 0.03$; Figure 3C). Interestingly, the lower activation of the DG observed in tested m266-treated Tg mice was associated with lower activation of the upper blade compared to tested vehicle-treated Tg mice (Egr-1$^+$ cell density in m266-treated Tg mice: 32.1 ± 3.8, and in vehicle-treated Tg mice: 50.8 ± 5.5; MW: $U = 2.0$, $Z = 2.2$, $P = 0.03$; Figure 3C and Table S1). Thus, the behavioral task activated the upper blade of the GCL in mice, while m266 treatment selectively limited this activation in Tg mice.

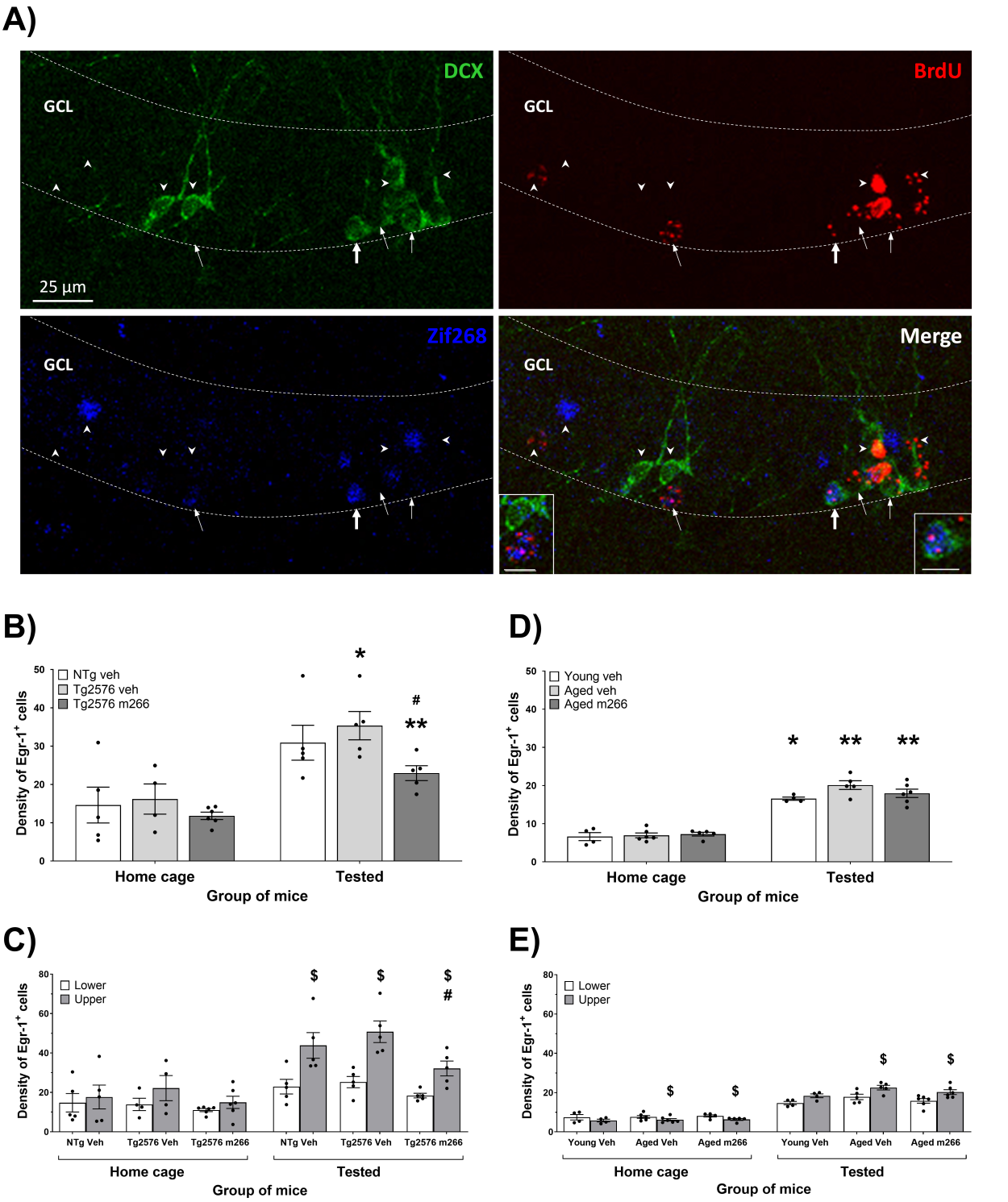

Figure 3. Pattern separation task induces a global activation of the dorsal GCL in 5-month-old Tg2576 and aged C57BL/6J mice. (**A**) Representative micrographs of triple immunostained sections for DCX (D, green), BrdU (B, red), and Egr-1 (Zif268) (E, blue). Brains were collected in HC mice and tested mice 90 min after PS testing. The GCL is delineated by the white dot lines. An example of a 4-week-old activated immature neuron (D+B+E+) is shown with a thick arrow and in the right inset. Double immunostained cells are shown with a smaller arrow for D+B+ (4-week-old immature neurons) and for B+E+ (4-week-old activated cells) and in the left inset. Finally, simple immunostained cells are shown with an arrowhead for B+ (4-week-old cells), D+ (immature neurons), or E+ (activated cells). GCL: granule cell layer. Scale bar in inset: 10 µm. (**B**) and (**D**) Effect of a spatial PS task on the mean density (± SEM) of Egr-1$^+$ cells counted per 10^6 µm^3 GCL for Tg mice, and aged mice, respectively (n = 4–6/group, see Table S1). Data were analyzed using a non-parametric test: Mann-Whitney (MW)/Kruskal-Wallis: * $P < 0.05$ and ** $P < 0.01$ compared to their respective home cage group, $^\#$ $P < 0.05$ compared to tested Tg2576 vehicle (veh). (**C**) and (**E**) The PS-induced activation of granule cells was higher in the upper blade than in the lower blade in tested Tg and B6 mice, respectively. Data were analyzed using non-parametric tests: MW: $^\#$ $P < 0.05$ compared to the upper blade of veh groups (Tg2576) and Wilcoxon: $^\$$ $P < 0.05$ compared to the lower blade of a same group. DCX: doublecortin; HC: home cage

In the aging experiment, the density of Egr-1+ cells in the GCL was significantly higher in tested groups than in HC groups (pooled tested mice: 18.2 ± 1.0 cells, pooled HC mice: 6.9 ± 0.2 cells; MW: $U = 0$, $Z = -4.7$, $P < 0.0001$; Figure 3D, Table S1, and Figure S3), a result comparable to the one observed in the Tg experiment. The level of activated cells was similar among the three HC groups (KW: $H = 0.2$, $P = 0.9$) and among the three tested groups (KW: $H = 3.8$; $P = 0.15$; Figure 3D). The increased number of activated cells in the GCL of tested mice was more pronounced in the upper blade (upper: 20.5 ± 0.8 cells, lower: 16.1 ± 0.7 cells; pooled tested mice W: $Z = 3.4$, $P < 0.001$, Table S1) whereas, contrary to the Tg experiment, the lower blade was more active in HC group in B6 mice (pooled groups: W: $Z = 3.4$, $P < 0.001$; Figure 3E). For each group, the difference in activation between upper and lower blade was significant only in aged B6 groups (vehicle-treated aged mice W: $Z = 2.0$, $P < 0.05$, m266-treated aged mice: W: $Z = 2.2$, $P < 0.05$; young mice W: $Z = 1.5$, $P > 0.10$). There was no effect of the m266 treatment on task-induced GCL activation in the aged groups in either blade. Thus, the behavioral task induced a similar global activation of the GCL regardless of group and treatment.

Survival and phenotype of 4-week-old cells in the GCL of Tg mice

About one third of adult-born neurons survive up to one month [56] and neurogenesis is thought to be involved in PS performance. Thus, using BrdU injections, we labeled cells born ($BrdU^+$) a few days after passive immunization began (Figure 2A) in order to quantify them one month after PS completion in tested groups or their control (HC) counterparts. This quantification was carried out only in the Tg experiment since aged B6 mice showed dramatically reduced levels of neurogenesis in the GCL [29]. The density of $BrdU^+$ cells was stable among groups and conditions (two to three cells/0.001 mm^3 GCL; Figure 4A and Table S2). There were significantly more $BrdU^+$ cells in the upper blade than in the lower blade regardless of group and condition [pooled mice (mean ± SEM), lower: 2.6 ± 0.2 and upper: 4.0 ± 0.3, W: $Z = 4.8$, $P < 0.00001$; pooled tested mice for lower: 2.6 ± 0.3 and upper: 3.9 ± 0.4, W: $Z = 3.4$, $P < 0.001$; pooled HC mice for lower: 2.7 ± 0.2 and upper: 4.0 ± 0.3, W: $Z = 3.4$, $P < 0.001$, see Table S2]. In addition, there were no significant differences between groups for the lower blade or for the upper blade, regardless of behavioral conditions. Thus, the survival of 4-week-old cells in both DG blades was not affected by the behavioral task, the genotype, or the m266 treatment in Tg mice.

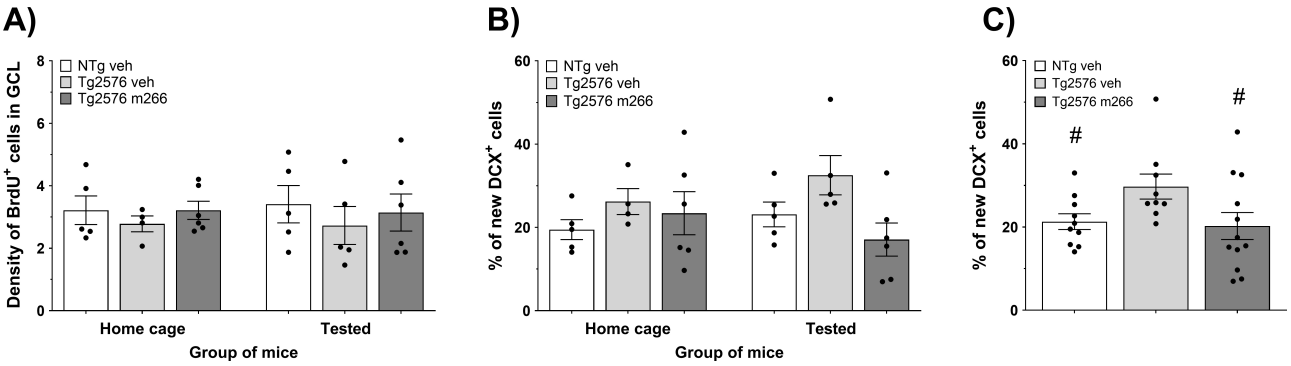

Figure 4. Effect of m266 on survival and phenotype of newly generated cells in the GCL of Tg2576 mice. (**A**) The density of $BrdU^+$ cells was not significantly altered between groups (n = 4–6/group, see Table S2). (**B**) The percentage of newborn DCX^+ cells among total $BrdU^+$ cells tended to be higher in vehicle (veh)-treated Tg2576 mice. (**C**) Pooled behavioral condition (HC and PS-tested mice) for the percentage of newborn DCX^+ cells among total $BrdU^+$ cells showed a significant increase of immature new neurons in veh-treated Tg2576 mice. Data are expressed as the mean density (± SEM) of total $BrdU^+$ cells/0.001 mm^3 GCL or as the percentage of $BrdU^+$ cells, and were analyzed with non-parametric tests. MW: $^{\#}P < 0.05$ compared to tested Tg2576 veh. DCX: doublecortin; GCL: granule cell layer; HC: home cage; PS: pattern separation

We further evaluated the percentage of four-week-old $BrdU^+$ cells expressing DCX protein (Figure 4B). This neuronal marker identifies new neuronal progenitors (around 8–15 days post birth) and new immature neurons (around 15–30 days post birth) [45, 46]. Thus, in our study, co-labeling of $BrdU^+/DCX^+$ was used to identify four-week-old immature neurons. There was no global effect of behavioral conditions on the percentage of new immature neurons in the GCL (pooled HC mice: 22.8 ± 2.3% and pooled tested mice: 23.8 ± 2.7%; MW test: $U = 110$, $Z = -0.4$, $P = 0.7$, Figure 4B and Table S3). However, in HC as in tested

groups, the vehicle-treated Tg mice tended to have more new immature neurons in the GCL than vehicle-treated NTg mice and m266-treated Tg mice (tested groups: KW test: $H = 5.8$, $P = 0.056$, MW: NTg vs vehicle-treated Tg mice: $U = 4$, $Z = -1.7$, $P = 0.095$, m266-treated Tg vs vehicle-treated Tg: $U = 4$, $Z = 1.9$, $P = 0.055$). We analyzed all three treated groups on pooled behavioral conditions. The population of immature neurons in the GCL was statistically larger in vehicle-treated Tg mice than in other groups (KW test: $H = 6.3$, $P = 0.04$, MW: vehicle-treated Tg vs vehicle-treated NTg: $U = 16$, $Z = -2.3$, $P = 0.02$, vehicle-treated Tg vs m266-treated Tg: $U = 26$, $Z = 2$, $P = 0.05$; Figure 4C). No differences were observed between vehicle-treated NTg and m266-treated mice (MW: NTg vs m266-treated Tg2576: $U = 50$, $Z = 0.7$, $P = 0.5$). Taken together, these results suggest that Tg mice displayed newer immature (DCX-positive) neurons than NTg mice, and that the m266 treatment tended to lower the density of new immature neurons to the same level as in NTg mice.

Interestingly, the upper blade displayed a significantly higher percentage of immature new neurons than the lower blade (pooled mice for lower blade: 20.4 ± 2% and upper blade: 25.3 ± 2.0%; W: $Z = 3$, $P = 0.003$, see Table S3). However, whatever the behavioral conditions, there only was a significant group effect in the lower blade (KW: upper, $H = 4.8$, $P = 0.09$ and lower, $H = 7.8$, $P = 0.02$, see Table S3). Indeed, vehicle-treated Tg mice exhibited significantly more new immature neurons in the lower blade compared to m266-treated Tg mice (MW lower blade: $Z = 2.5$, $P = 0.01$, MW upper blade: $Z = 1.8$, $P = 0.07$) and NTg mice (MW lower blade: $Z = -2.1$, $P = 0.03$, MW upper blade: $Z = -1.8$, $P = 0.08$). Thus, the m266 treatment of Tg mice lowered the percentage of immature neurons in the lower blade to the same level as in vehicle-treated NTg. These results suggest that vehicle-treated Tg mice displayed more new immature neurons than the other groups and that the m266 treatment restored a percentage of immature neurons similar to that of NTg mice.

Finally, statistical analysis of new neuron activation was not performed due to the very low percentage of new neurons expressing Egr-1 (pooled all groups: % of DCX^+ neurons: 1.4 ± 0.4%, see Table S4).

Quantification of Aβ levels in the CA3/DG region

After the four-week m266 passive immunization treatment against Aβ, we analyzed the total levels of human Aβ40 and Aβ42 in the CA3/DG region of vehicle-treated and m266-treated Tg female mice (n = 4–5/group, exclusion of one m266-treated Tg which was considered as an outlier), as well as the total levels of murine Aβ40 and Aβ42 in vehicle-treated young and aged B6 male mice (n = 4–6/group), and m266-treated aged B6 male mice (n = 4). In the Tg experiment, the total level of Aβ peptides (Aβ40 + Aβ42) in the CA3/DG region was slightly but not significantly lower in m266-treated Tg mice compared to vehicle-treated mice (m266 Tg, Aβ: 2,127 ± 133 pg/mg of tissue; vehicle Tg, Aβ: 2,736 ± 271 pg/mg of tissue; MW: $U = 7$, $Z = -1.4$, $P = 0.2$, Figure 5A and Table S5). As expected, the level of Aβ40 in young Tg2576 mice was significantly higher than that of Aβ42 whatever the treatment (W: vehicle-treated mice: $Z = 2.2$, $P = 0.03$; m266-treated mice: $Z = 2.0$, $P = 0.04$, Table S5). The ratio of Aβ42 to Aβ40 remained stable among Tg groups (Figure 5A, Table S5). In the aging experiment, the total level of Aβ peptides remained stable among groups (young B6, Aβ: 486.3 ± 76.8 pg/mg of tissue; m266 old B6, Aβ: 456.7 ± 82.65 pg/mg of tissue; vehicle old B6, Aβ: 380.2 ± 74.5 pg/mg of tissue, Figure 5B and Table S5), with a higher level of Aβ40 compared to Aβ42 (W, vehicle-treated young B6: $Z = 2.2$, $P = 0.03$, vehicle-treated aged B6: $Z = 2.2$, $P = 0.03$) except in m266-treated aged B6 ($Z = 1.8$, $P = 0.07$, see Table S5). The ratio of Aβ42 to Aβ40 in aged mice was not significantly different from the one in young mice (vehicle-treated young B6: 0.3 ± 0.04, vehicle-treated aged B6: 0.4 ± 0.02, m266-treated aged B6: 0.4 ± 0.03, Figure 5B and Table S5). As expected, the total level of human Aβ peptides in Tg mice (mean of vehicle- and treated-mice: 2,459 ± 180.3 pg/mg of tissue) was much higher than that of murine Aβ peptides in young (486.3 ± 76.8 pg/mg of tissue) and aged B6 mice (mean of vehicle- and treated-mice: 410.8 ± 54.0 pg/mg of tissue). Thus, the m266 treatment only had marginal effect on Aβ levels in CA3/DG of 5-month-old Tg mice, and B6 mice.

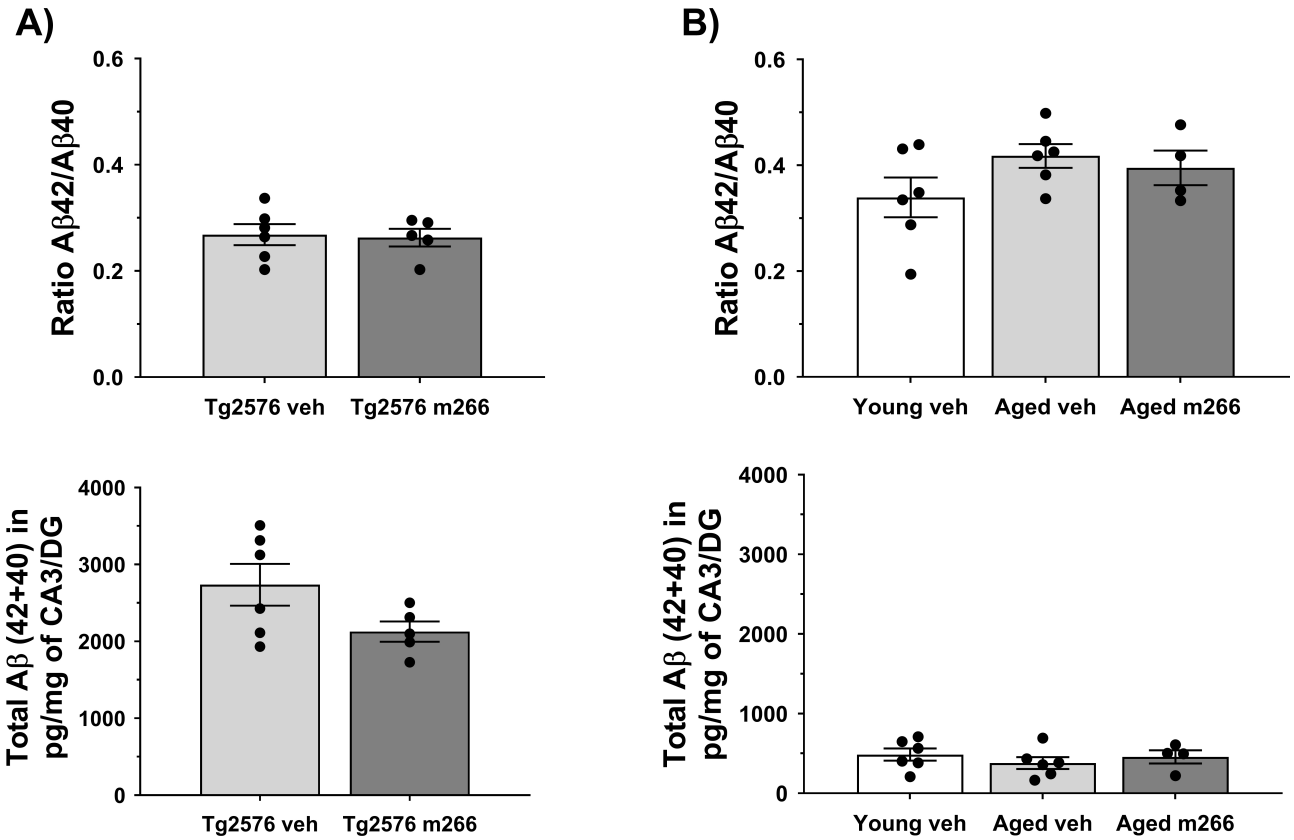

Figure 5. Level of Aβ in the DG/CA3 region of Tg2576 and C57BL6/J mice. Ratio of Aβ42/Aβ40 and total level of Aβ (40 + 42) were measured in the DG/CA3 of Tg2576 mice (**A**) and C57BL6/J mice (**B**). Histograms represent mean (± SEM) for each group of mice. Tg2576 data were analyzed with a Mann-Whitney test whereas old mice data were analyzed by a Kruskal-Wallis test. DG: dentate gyrus; veh: vehicle

Discussion

Aging and AD are known to alter PS early in humans and rodents [9, 10, 29–31, 57–59]. In this study, we first evaluated the spatial PS deficits in Tg2576 and aged C57BL/6J mice, and we then tested passive immunotherapy targeting Aβ peptides to determine the contribution of Aβ in this early cognitive deficit. We further analyzed neuronal activity using a molecular tracer (Egr-1 expression) and the survival of adult-born neurons to test whether neurogenesis was involved in any potential beneficial effects of the treatment. We will now discuss the origin of the PS dysfunction in the two mouse models.

Herein, we showed that female Tg mice display a spatial PS deficit as early as 4 months of age and that following a four-week treatment with m266, an Aβ neutralizer, this deficit was no longer observed. Thus, these results support the hypothesis that PS deficits are in fact produced by the emerging amyloid pathology. Interestingly, a similar impairment in aged B6 male mice was not prevented by m266, suggesting that these deficits may have a different neurobiological origin than in Tg mice. However, one might suggest that the m266 treatment was administered too late or too briefly to have beneficial effects in aged mice. The lack of increase in CA3/DG Aβ levels argues against this hypothesis and supports an Aβ-independent deficit. Notably, m266 did not impact reduced exploration observed in five-month-old Tg mice, suggesting that both PS deficits and the beneficial effect of passive immunotherapy on their performance were associated with their ability to explore objects.

The increase in Egr-1 expression within the GCL of all tested groups would be in line with the key role of the DG in PS function [60, 61]. However, in our study, this task-dependent neuronal activation also occurred in NTg and young B6 mice as well as in Tg and aged B6 mice, even those presenting an impairment of the spatial PS task. Thus, the activation of DG granule cells appears to be related to the behavioral testing experiment rather than the effectiveness of PS.

In agreement with the fact that the upper blade was found more active in our study, it was reported in rats that upper blade neurons have a greater dendritic length and spine density, notably at inputs from the entorhinal cortex, compared to the lower blade, and are thus more active during spatial tasks than in lower blade [62, 63]. This may suggest that impaired spatial PS observed in Tg and aged B6 mice may involve alteration of downstream structures, such as the CA3 region, rather than in the DG or entorhinal inputs. Of note, it was shown that the upper blade receives more projections from the lateral entorhinal cortex (LEC) which is associated with object information processing in human, while the lower blade receives more projections from the medial entorhinal cortex (MEC) which is associated with spatial information processing [64, 65]. As each blade of the GCL had a similar level of neuronal activation among all groups of mice, neither MEC nor LEC projections to the DG of five-month-old Tg or of aged B6 mice appear to be impaired.

Surprisingly, m266-treated Tg mice had a significantly reduced number of activated neurons in the DG compared to vehicle-treated Tg mice, in particular in the upper blade. This result suggests that a reduced activation in the upper blade could improve performance in the PS task, and that the passive immunotherapy could normalize contribution of the DG to memory recall in the PS test. The mechanisms underlying this reduced activation and how it results in improved efficiency in the PS test remain unclear. In accordance with this, Alcantara-Gonzalez et al. [66, 67] and Kim et al. [31] found that young Tg2576 mice exhibit hyperexcitability of granule and mossy cells. Moreover, Xu et al. [68] showed LEC hyperactivity (main inputs of the upper blade) in three and six-month-old Tg2576 mice associated with an increase of AβPP-C terminal fragment and soluble Aβ peptides in entorhinal cortex and hippocampus. As the inputs from the LEC are one of the main entries to the upper blade of the DG, it is possible that our vehicle-treated Tg mice exhibited early abnormal activity in their LEC. This abnormal activity could spread either to the DG, disrupting its function without significantly altering its neuronal activation compared to NTg mice, or directly in the CA2 region, which receives direct excitatory input from the LEC [69]. In both cases, the functionality of the downstream CA1 region would likely be altered. In addition, Shah et al. [70] showed a hypersynchrony of functional connectivity in the hippocampal network and synaptic impairments in 5-month-old Tg2576 that were rescued by an anti-Aβ (3D6) passive immunotherapy. Therefore, the Aβ-induced impairment of PS in our 5-month-old Tg could be due to abnormal activity in entorhinal cortex and/or the DG, which could be normalized by m266 passive immunotherapy.

In tested B6 mice, all groups displayed an increased neuronal activation upon PS testing whatever the DG blades when compared to their HC controls. However, the difference in neuronal activation between the two GCL blades was only statistically significant in aged B6 mice, the upper blade showing more Egr-1 positive cells than the lower blade, suggesting that overactivation in the upper blade could alter the performance in the PS task. Similarly, PS deficits in healthy elderly human has been associated with an increased activity of the CA3/DG regions [8, 71]. However, the m266 passive immunotherapy failed to reduce this difference in neuronal activation between GCL blades in aged B6 mice. Thus, these results suggest that the PS deficiency in aged mice involves different neurobiological mechanisms than those in Tg mice, leading in both cases to overactivation of the upper blade of the DG. In old B6 mice, these mechanisms would be triggered by aging, whereas in Tg mice, Aβ-dependent mechanisms would be sufficient to promote upper blade activation. Taken together, these data suggest a critical role of the upper blade in the ability of the DG to discriminate similar spatial information.

The success of passive immunotherapy in Tg mice only suggests that the Aβ environment may be responsible for the PS impairment and that m266 treatment inactivated a sufficiently large pool of Aβ to rescue this deficit. The beneficial effect of the m266 treatment was observed despite the fact that the decrease of Aβ level was low in the CA3/DG region of m266-treated mice compared to vehicle-treated Tg mice. It has already been shown in 24-month-old PDAPP mice that a six weeks passive immunization with m266 rescued performance in an object recognition task without reduction of Aβ deposition in the brain [40]. Although a much longer m266 treatment does reduce amyloid burden in this model, the m266 antibody was shown to sequester soluble forms of Aβ, rather than deposits [35]. Previous works showed that there is a poor correlation between β-amyloid plaques and cognitive deficits in AD patients and mouse

models [72, 73] while others showed a positive correlation [74, 75]. However, Tg does not display amyloid plaques nor insoluble Aβ before six months of age [76]. Thus, we assume that our passive immunotherapy alleviated PS deficits in younger Tg through sequestration of soluble Aβ peptides in their brain, leading to brain preservation from negative Aβ effects without decreasing total cerebral Aβ levels measured in our ELISA assays. Indeed, soluble Aβ is known to induce neuronal dysfunction through different mechanisms [77, 78] such as disruption of synaptic glutamatergic [79, 80] or cholinergic receptors/transmission [81, 82]. Soluble Aβ seems more toxic and responsible for long-term potentiation alteration [83] or synaptic impairment in mouse models of AD [84]. Thus, preventing interactions of soluble Aβ with synaptic receptors through their binding to m266 may prevent disruption of synaptic plasticity involved in learning and memory process. In conclusion, our findings indicate that soluble Aβ species are most responsible for PS dysfunction in 4- to 5-month-old Tg2576 mice. Our interpretation is coherent with studies showing that soluble Aβ species correlate more strongly with the severity of the disease [85] and dementia [86, 87] than insoluble species in AD patients.

Interestingly, we found no effect of amyloid pathology, nor of the PS task or m266 treatment, on the density of newly born $BrdU^+$ cells surviving in the DG of Tg mice. Among these surviving cells, the percentage of immature four-week-old neurons ($BrdU^+$ DCX^+ cells) was significantly higher in vehicle-treated Tg mice than in NTg controls or in m266-treated Tg mice, indicating that m266 treatment lowered the excessive density of immature neurons observed in the GCL of Tg mice. This suggests that high level of Aβ altered neuronal maturation in the Tg mouse DG, either during the "progenitors to immature neurons" transition (increase) or during the "immature neurons to mature neurons" transition (decrease), which would have contributed to PS dysfunction. Thus, treatment with m266 seems to not only have restored PS function but also normalized the level of immature neurons in Tg mice, probably by protecting the neuronal maturation. It was previously shown that APPxPS1, a mouse model of amyloidopathy, displayed an impaired differentiation of new neurons [88]. Moreover, Krezymon et al. [89] showed that 5-month-old Tg mice exhibited fewer neuronal progenitors ($BrdU^+/DCX^+/NeuN^-$) and no change in mature new neurons ($BrdU^+/DCX^-/NeuN^+$) in the GCL compared to NTg mice, but they did not evaluate the number of 4-week-old immature neurons ($BrdU^+/DCX^+/NeuN^+$). These results argue for an increase of 4-week-old immature neurons as found in our study. The effect of m266 treatment on the immature four-week-old neurons was observed in both blades of the GCL of Tg mice, with an emphasis on the lower blade. It receives more projections from the MEC, one of the brain structures processing the spatial information [64, 65]. Thus, m266 treatment may have mainly rescued the ability of the DG to process spatial information by significantly reducing the level of immature neurons in the lower blade and, in counterbalance, enhancing the number of mature ones. Interestingly, it was shown that adult-born immature neurons had an enhanced excitability compared to adult-born mature neurons [90]. Moreover, McHugh et al. [91] have shown that selective activation of four to seven-week-old adult-born GCs increases the dentate network sparsity. By contrast, silencing of this GC population reduces sparsity and leads to impaired object recognition. Thus, four-week m266 treatment in the present study could have normalized sparsity of the dentate network and PS performance of Tg mice by restoring the maturation of (four-week-old) adult-born neurons.

The lack of effects of m266 treatment on spatial PS performance in aged B6 mice suggests that Aβ was not involved in their PS impairment. In addition, the quantification of Aβ peptides in the CA3/DG regions showed that young B6 mice displaying a similar Aβ level as old B6 mice performed well in the PS task. In Cès et al. [29], we have already showed that 18-month-old B6 mice displayed PS deficits and very few four-week-old adult-born cells in the GCL compared to three-month-old B6 mice. Here, as m266 treatment did not to restore PS function in 20-month-old B6 mice, we did not analyze the few rare adult-born neurons in the DG of 20-month-old B6 mice. Interestingly, in this previous study, we were able to rescue the PS deficit in aged B6 mice with a one-week D-serine treatment, which had a very faint effect on the number of four-week-old adult-born neurons. D-serine, a co-agonist of NMDA receptors and mainly produced by neurons and astrocytes, is drastically decreased in the hippocampus of learning and memory-impaired aged rats [92]. Therefore, by restoring the regulation of the NMDA receptors, D-serine could restore normal neuronal activity in the upper blade of aged B6 mice. Thus, aging-dependent impairments of other neurobiological mechanisms than the decrease in adult neurogenesis could be involved in the PS deficit of aged B6 mice.

To conclude, we showed that PS impairment during a prodromal stage of AD could be rescued by Aβ passive immunotherapy, which was not the case in an aging mouse model. Our data suggested a different neurobiological origin of this PS deficit in AD compared to normal aging, leading to an overactivation of the GCL upper blade. We also identified an increase in immature 4-week-old adult-born neurons in Tg mice which was associated with impaired PS, despite poor recruitment during the PS task. Thus, our findings support Aβ passive immunotherapy to prevent earlier cognitive deficits/prodromal stage of AD and the necessity to further investigate the mechanism underlying the age-dependent PS deficits in order to find new treatments.

Abbreviations

AD: Alzheimer's disease

Aβ: β-amyloid peptide

CA3: Ammon's horn 3

DCX: doublecortin

DG: dentate gyrus

GCL: granular cell layer

HC: home cage

IP: intraperitoneal

KW: Kruskal-Wallis

LEC: lateral entorhinal cortex

MEC: medial entorhinal cortex

MW: Mann-Whitney

NTg: non-transgenic

PBS: phosphate-buffered saline

PS: Pattern separation

Tg: Tg2576 mice

W: Wilcoxon test

WSR: Wilcoxon signed rank test

Supplementary materials

The supplementary materials for this article are available at: https://www.explorationpub.com/uploads/Article/file/1004108_sup_1.pdf.

Declarations

Acknowledgments

The authors wish to thank Dr Cornelia Dorner-Ciossek and Dr Holger Rosenbrock from Boehringer Ingelheim (Biberach an der Riss, Germany) for kindly providing the m266 used in the present study. We also thank Olivier Bildstein and Georges Egesi for taking care of our mice. The authors thank the "Plateforme Imagerie in Vitro" at the Center of Neurochemistry (INCI) and the INCI for the In Vitro imaging platform (Strasbourg, France) for the confocal microscope (Leica SP5 II). Finally, the authors thank Vincent Loizeau for his help with language editing.

Author contributions

KH: Investigation, Resources, Formal analysis. CB: Investigation, Formal analysis. C Mursch: Investigation, Formal analysis. VK: Resources. OB: Resources. ALB: Writing—original draft, Writing—review & editing. C

Mathis: Conceptualization, Funding acquisition, Methodology, Investigation, Formal analysis, Project administration, Resources, Supervision, Validation, Visualization, Writing—original draft, Writing—review & editing. CH: Conceptualization, Investigation, Methodology, Formal analysis, Project administration, Resources, Supervision, Validation, Visualization, Writing—original draft, Writing—review & editing.

Conflicts of interest

The authors declare that they have no conflicts of interest.

Ethical approval

All procedures were performed in accordance to the European Directive (2010/63UE) and were approved by the local ethical committee (Comité Régional d'Ethique en Matière d'Expérimentation Animale de Strasbourg CEEA 35, reference # 02965.02).

Consent to participate

Not applicable.

Consent to publication

Not applicable.

Availability of data and materials

The datasets that support the findings of this study are available from the corresponding author upon reasonable request.

Funding

This work was co-funded by the Association France Alzheimer et Maladies Apparentées and the group Intériale. Additional support was provided by the University of Strasbourg and the Centre National de la Recherche Scientifique (CNRS). All these funding sources had no involvement in any aspect of the study design, in the collection, analysis and interpretation of data, in the writing of the report and in the decision to submit the article for publication.

Publisher's note

Open Exploration maintains a neutral stance on jurisdictional claims in published institutional affiliations and maps. All opinions expressed in this article are the personal views of the author(s) and do not represent the stance of the editorial team or the publisher.

References

1. Bateman RJ, Xiong C, Benzinger TLS, Fagan AM, Goate A, Fox NC, et al. Clinical and biomarker changes in dominantly inherited Alzheimer's disease. N Engl J Med. 2012;367:795–804. [DOI] [PubMed] [PMC]
2. Selkoe DJ. Preventing Alzheimer's disease. Science. 2012;337:1488–92. [DOI] [PubMed]
3. Hou Y, Dan X, Babbar M, Wei Y, Hasselbalch SG, Croteau DL, et al. Ageing as a risk factor for neurodegenerative disease. Nat Rev Neurol. 2019;15:565–81. [DOI] [PubMed]
4. Yeung L, Olsen RK, Hong B, Mihajlovic V, D'Angelo MC, Kacollja A, et al. Object-in-place Memory Predicted by Anterolateral Entorhinal Cortex and Parahippocampal Cortex Volume in Older Adults. J Cogn Neurosci. 2019;31:711–29. [DOI] [PubMed]
5. Didic M, Barbeau EJ, Felician O, Tramoni E, Guedj E, Poncet M, et al. Which memory system is impaired first in Alzheimer's disease? J Alzheimers Dis. 2011;27:11–22. [DOI] [PubMed]

6. Petok JR, Myers CE, Pa J, Hobel Z, Wharton DM, Medina LD, et al. Impairment of memory generalization in preclinical autosomal dominant Alzheimer's disease mutation carriers. Neurobiol Aging. 2018;65:149–57. [DOI] [PubMed] [PMC]
7. Marr D, Willshaw D, McNaughton B. Simple Memory: A Theory for Archicortex. In: Vaina L, editor. From the Retina to the Neocortex. Boston: Birkhäuser; 1991. pp. 59–128. [DOI]
8. Yassa MA, Stark SM, Bakker A, Albert MS, Gallagher M, Stark CEL. High-resolution structural and functional MRI of hippocampal CA3 and dentate gyrus in patients with amnestic Mild Cognitive Impairment. Neuroimage. 2010;51:1242–52. [DOI] [PubMed] [PMC]
9. Stark SM, Yassa MA, Stark CEL. Individual differences in spatial pattern separation performance associated with healthy aging in humans. Learn Mem. 2010;17:284–8. [DOI] [PubMed] [PMC]
10. Stark SM, Yassa MA, Lacy JW, Stark CEL. A task to assess behavioral pattern separation (BPS) in humans: Data from healthy aging and mild cognitive impairment. Neuropsychologia. 2013;51:2442–9. [DOI] [PubMed] [PMC]
11. Reagh ZM, Roberts JM, Ly M, DiProspero N, Murray E, Yassa MA. Spatial discrimination deficits as a function of mnemonic interference in aged adults with and without memory impairment. Hippocampus. 2014;24:303–14. [DOI] [PubMed] [PMC]
12. Yassa MA, Muftuler LT, Stark CEL. Ultrahigh-resolution microstructural diffusion tensor imaging reveals perforant path degradation in aged humans in vivo. Proc Natl Acad Sci U S A. 2010;107: 12687–91. [DOI] [PubMed] [PMC]
13. Gilbert PE, Kesner RP, DeCoteau WE. Memory for spatial location: role of the hippocampus in mediating spatial pattern separation. J Neurosci. 1998;18:804–10. [DOI] [PubMed] [PMC]
14. Goodrich-Hunsaker NJ, Hunsaker MR, Kesner RP. The interactions and dissociations of the dorsal hippocampus subregions: how the dentate gyrus, CA3, and CA1 process spatial information. Behav Neurosci. 2008;122:16–26. [DOI] [PubMed]
15. Jung MW, McNaughton BL. Spatial selectivity of unit activity in the hippocampal granular layer. Hippocampus. 1993;3:165–82. [DOI] [PubMed]
16. Leutgeb JK, Leutgeb S, Moser M, Moser EI. Pattern separation in the dentate gyrus and CA3 of the hippocampus. Science. 2007;315:961–6. [DOI] [PubMed]
17. Neunuebel JP, Knierim JJ. CA3 retrieves coherent representations from degraded input: direct evidence for CA3 pattern completion and dentate gyrus pattern separation. Neuron. 2014;81:416–27. [DOI] [PubMed] [PMC]
18. Jain S, Yoon SY, Zhu L, Brodbeck J, Dai J, Walker D, et al. Arf4 determines dentate gyrus-mediated pattern separation by regulating dendritic spine development. PLoS One. 2012;7:e46340. [DOI] [PubMed] [PMC]
19. Tronel S, Belnoue L, Grosjean N, Revest J, Piazza P, Koehl M, et al. Adult-born neurons are necessary for extended contextual discrimination. Hippocampus. 2012;22:292–8. [DOI] [PubMed]
20. McHugh TJ, Jones MW, Quinn JJ, Balthasar N, Coppari R, Elmquist JK, et al. Dentate gyrus NMDA receptors mediate rapid pattern separation in the hippocampal network. Science. 2007;317:94–9. [DOI] [PubMed]
21. Bolz L, Heigele S, Bischofberger J. Running Improves Pattern Separation during Novel Object Recognition. Brain Plast. 2015;1:129–41. [DOI] [PubMed] [PMC]
22. Nakashiba T, Cushman JD, Pelkey KA, Renaudineau S, Buhl DL, McHugh TJ, et al. Young dentate granule cells mediate pattern separation, whereas old granule cells facilitate pattern completion. Cell. 2012;149:188–201. [DOI] [PubMed] [PMC]
23. Sahay A, Scobie KN, Hill AS, O'Carroll CM, Kheirbek MA, Burghardt NS, et al. Increasing adult hippocampal neurogenesis is sufficient to improve pattern separation. Nature. 2011;472:466–70. [DOI] [PubMed] [PMC]

24. Clelland CD, Choi M, Romberg C, Clemenson GD Jr, Fragniere A, Tyers P, et al. A functional role for adult hippocampal neurogenesis in spatial pattern separation. Science. 2009;325:210–3. [DOI] [PubMed] [PMC]
25. Burke SN, Wallace JL, Nematollahi S, Uprety AR, Barnes CA. Pattern separation deficits may contribute to age-associated recognition impairments. Behav Neurosci. 2010;124:559–73. [DOI] [PubMed] [PMC]
26. Gracian EI, Shelley LE, Morris AM, Gilbert PE. Age-related changes in place learning for adjacent and separate locations. Neurobiol Aging. 2013;34:2304–9. [DOI] [PubMed] [PMC]
27. Johnson SA, Turner SM, Santacroce LA, Carty KN, Shafiq L, Bizon JL, et al. Rodent age-related impairments in discriminating perceptually similar objects parallel those observed in humans. Hippocampus. 2017;27:759–76. [DOI] [PubMed] [PMC]
28. Creer DJ, Romberg C, Saksida LM, Praag Hv, Bussey TJ. Running enhances spatial pattern separation in mice. Proc Natl Acad Sci U S A. 2010;107:2367–72. [DOI] [PubMed] [PMC]
29. Cès A, Burg T, Herbeaux K, Héraud C, Bott J, Mensah-Nyagan AG, et al. Age-related vulnerability of pattern separation in C57BL/6J mice. Neurobiol Aging. 2018;62:120–9. [DOI] [PubMed]
30. Zhu H, Yan H, Tang N, Li X, Pang P, Li H, et al. Impairments of spatial memory in an Alzheimer's disease model via degeneration of hippocampal cholinergic synapses. Nat Commun. 2017;8:1676. [DOI] [PubMed] [PMC]
31. Kim K, Kim Y, Jeong H, Kang J, Lee SH, Kim Y, et al. Impaired pattern separation in Tg2576 mice is associated with hyperexcitable dentate gyrus caused by Kv4.1 downregulation. Mol Brain. 2021;14:62. [DOI] [PubMed] [PMC]
32. Rechnitz O, Slutsky I, Morris G, Derdikman D. Hippocampal sub-networks exhibit distinct spatial representation deficits in Alzheimer's disease model mice. Curr Biol. 2021;31:3292–302.e6. [DOI] [PubMed]
33. Gephine L, Roux CM, Freret T, Boulouard M, Leger M. Vulnerability of Spatial Pattern Separation in 5xFAD Alzheimer's Disease Mouse Model. J Alzheimers Dis. 2024;97:1889–900. [DOI] [PubMed]
34. Hsiao K, Chapman P, Nilsen S, Eckman C, Harigaya Y, Younkin S, et al. Correlative memory deficits, Abeta elevation, and amyloid plaques in transgenic mice. Science. 1996;274:99–102. [DOI] [PubMed]
35. DeMattos RB, Bales KR, Cummins DJ, Dodart JC, Paul SM, Holtzman DM. Peripheral anti-A beta antibody alters CNS and plasma A beta clearance and decreases brain A beta burden in a mouse model of Alzheimer's disease. Proc Natl Acad Sci U S A. 2001;98:8850–5. [DOI] [PubMed] [PMC]
36. Gallo FT, Katche C, Morici JF, Medina JH, Weisstaub NV. Immediate Early Genes, Memory and Psychiatric Disorders: Focus on c-Fos, Egr1 and Arc. Front Behav Neurosci. 2018;12:79. [DOI] [PubMed] [PMC]
37. Veyrac A, Gros A, Bruel-Jungerman E, Rochefort C, Borgmann FBK, Jessberger S, et al. *Zif268/egr1* gene controls the selection, maturation and functional integration of adult hippocampal newborn neurons by learning. Proc Natl Acad Sci U S A. 2013;110:7062–7. [DOI] [PubMed] [PMC]
38. Gouveia K, Hurst JL. Reducing mouse anxiety during handling: effect of experience with handling tunnels. PLoS One. 2013;8:e66401. [DOI] [PubMed] [PMC]
39. Ennaceur A, Neave N, Aggleton JP. Spontaneous object recognition and object location memory in rats: the effects of lesions in the cingulate cortices, the medial prefrontal cortex, the cingulum bundle and the fornix. Exp Brain Res. 1997;113:509–19. [DOI] [PubMed]
40. Dodart J, Bales KR, Gannon KS, Greene SJ, DeMattos RB, Mathis C, et al. Immunization reverses memory deficits without reducing brain Abeta burden in Alzheimer's disease model. Nat Neurosci. 2002;5:452–7. [DOI] [PubMed]
41. Brown JP, Couillard-Després S, Cooper-Kuhn CM, Winkler J, Aigner L, Kuhn HG. Transient expression of doublecortin during adult neurogenesis. J Comp Neurol. 2003;467:1–10. [DOI] [PubMed]
42. Snyder JS, Choe JS, Clifford MA, Jeurling SI, Hurley P, Brown A, et al. Adult-born hippocampal neurons are more numerous, faster maturing, and more involved in behavior in rats than in mice. J Neurosci. 2009;29:14484–95. [DOI] [PubMed] [PMC]

43. Rao MS, Shetty AK. Efficacy of doublecortin as a marker to analyse the absolute number and dendritic growth of newly generated neurons in the adult dentate gyrus. Eur J Neurosci. 2004;19:234–46. [DOI] [PubMed]
44. Couillard-Despres S, Winner B, Schaubeck S, Aigner R, Vroemen M, Weidner N, et al. Doublecortin expression levels in adult brain reflect neurogenesis. Eur J Neurosci. 2005;21:1–14. [DOI] [PubMed]
45. Encinas JM, Vaahtokari A, Enikolopov G. Fluoxetine targets early progenitor cells in the adult brain. Proc Natl Acad Sci U S A. 2006;103:8233–8. [DOI] [PubMed] [PMC]
46. Aguilar-Arredondo A, Arias C, Zepeda A. Evaluating the functional state of adult-born neurons in the adult dentate gyrus of the hippocampus: from birth to functional integration. Rev Neurosci. 2015;26: 269–79. [DOI] [PubMed]
47. Clark PJ, Bhattacharya TK, Miller DS, Rhodes JS. Induction of c-Fos, Zif268, and Arc from acute bouts of voluntary wheel running in new and pre-existing adult mouse hippocampal granule neurons. Neuroscience. 2011;184:16–27. [DOI] [PubMed] [PMC]
48. Huckleberry KA, Kane GA, Mathis RJ, Cook SG, Clutton JE, Drew MR. Behavioral experience induces zif268 expression in mature granule cells but suppresses its expression in immature granule cells. Front Syst Neurosci. 2015;9:118. [DOI] [PubMed] [PMC]
49. Snyder JS, Clifford MA, Jeurling SI, Cameron HA. Complementary activation of hippocampal-cortical subregions and immature neurons following chronic training in single and multiple context versions of the water maze. Behav Brain Res. 2012;227:330–9. [DOI] [PubMed] [PMC]
50. Jessberger S, Kempermann G. Adult-born hippocampal neurons mature into activity-dependent responsiveness. Eur J Neurosci. 2003;18:2707–12. [DOI] [PubMed]
51. Soulé J, Penke Z, Kanhema T, Alme MN, Laroche S, Bramham CR. Object-place recognition learning triggers rapid induction of plasticity-related immediate early genes and synaptic proteins in the rat dentate gyrus. Neural Plast. 2008;2008:269097. [DOI] [PubMed] [PMC]
52. Penke Z, Morice E, Veyrac A, Gros A, Chagneau C, LeBlanc P, et al. Zif268/Egr1 gain of function facilitates hippocampal synaptic plasticity and long-term spatial recognition memory. Philos Trans R Soc Lond B Biol Sci. 2013;369:20130159. [DOI] [PubMed] [PMC]
53. Schauwecker PE. Genetic influence on neurogenesis in the dentate gyrus of two strains of adult mice. Brain Res. 2006;1120:83–92. [DOI] [PubMed]
54. Schneider CA, Rasband WS, Eliceiri KW. NIH Image to ImageJ: 25 years of image analysis. Nat Methods. 2012;9:671–5. [DOI] [PubMed] [PMC]
55. Franklin KBJ, Paxinos G. The Mouse Brain in Stereotaxic Coordinates, Compact. 3rd ed. Academic Press; 2008.
56. van Praag H, Schinder AF, Christie BR, Toni N, Palmer TD, Gage FH. Functional neurogenesis in the adult hippocampus. Nature. 2002;415:1030–4. [DOI] [PubMed] [PMC]
57. Yassa MA, Lacy JW, Stark SM, Albert MS, Gallagher M, Stark CEL. Pattern separation deficits associated with increased hippocampal CA3 and dentate gyrus activity in nondemented older adults. Hippocampus. 2011;21:968–79. [DOI] [PubMed] [PMC]
58. Wesnes KA, Annas P, Basun H, Edgar C, Blennow K. Performance on a pattern separation task by Alzheimer's patients shows possible links between disrupted dentate gyrus activity and apolipoprotein E ∈4 status and cerebrospinal fluid amyloid-β42 levels. Alzheimers Res Ther. 2014;6: 20. [DOI] [PubMed] [PMC]
59. Parizkova M, Lerch O, Andel R, Kalinova J, Markova H, Vyhnalek M, et al. Spatial Pattern Separation in Early Alzheimer's Disease. J Alzheimers Dis. 2020;76:121–38. [DOI] [PubMed]
60. Gilbert PE, Kesner RP, Lee I. Dissociating hippocampal subregions: double dissociation between dentate gyrus and CA1. Hippocampus. 2001;11:626–36. [DOI] [PubMed]
61. Hunsaker MR, Kesner RP. Evaluating the differential roles of the dorsal dentate gyrus, dorsal CA3, and dorsal CA1 during a temporal ordering for spatial locations task. Hippocampus. 2008;18:955–64. [DOI] [PubMed] [PMC]

62. Gallitano AL, Satvat E, Gil M, Marrone DF. Distinct dendritic morphology across the blades of the rodent dentate gyrus. Synapse. 2016;70:277–82. [DOI] [PubMed] [PMC]
63. Amaral DG, Scharfman HE, Lavenex P. The dentate gyrus: fundamental neuroanatomical organization (dentate gyrus for dummies). Prog Brain Res. 2007;163:3–22. [DOI] [PubMed] [PMC]
64. Schmidt B, Marrone DF, Markus EJ. Disambiguating the similar: the dentate gyrus and pattern separation. Behav Brain Res. 2012;226:56–65. [DOI] [PubMed]
65. Reagh ZM, Yassa MA. Object and spatial mnemonic interference differentially engage lateral and medial entorhinal cortex in humans. Proc Natl Acad Sci U S A. 2014;111:E4264–73. [DOI] [PubMed] [PMC]
66. Alcantara-Gonzalez D, Chartampila E, Criscuolo C, Scharfman HE. Early changes in synaptic and intrinsic properties of dentate gyrus granule cells in a mouse model of Alzheimer's disease neuropathology and atypical effects of the cholinergic antagonist atropine. Neurobiol Dis. 2021;152: 105274. [DOI] [PubMed] [PMC]
67. Alcantara-Gonzalez D, Kennedy M, Criscuolo C, Botterill J, Scharfman HE. Increased excitability of dentate gyrus mossy cells occurs early in life in the Tg2576 model of Alzheimer's disease. bioRxiv. 2024;2024.02.09.579729. [DOI] [PubMed] [PMC]
68. Xu W, Fitzgerald S, Nixon RA, Levy E, Wilson DA. Early hyperactivity in lateral entorhinal cortex is associated with elevated levels of AβPP metabolites in the Tg2576 mouse model of Alzheimer's disease. Exp Neurol. 2015;264:82–91. [DOI] [PubMed] [PMC]
69. Lopez-Rojas J, Solis CAd, Leroy F, Kandel ER, Siegelbaum SA. A direct lateral entorhinal cortex to hippocampal CA2 circuit conveys social information required for social memory. Neuron. 2022;110: 1559–72.e4. [DOI] [PubMed] [PMC]
70. Shah D, Praet J, Hernandez AL, Höfling C, Anckaerts C, Bard F, et al. Early pathologic amyloid induces hypersynchrony of BOLD resting-state networks in transgenic mice and provides an early therapeutic window before amyloid plaque deposition. Alzheimers Dement. 2016;12:964–76. [DOI] [PubMed]
71. Reagh ZM, Noche JA, Tustison NJ, Delisle D, Murray EA, Yassa MA. Functional Imbalance of Anterolateral Entorhinal Cortex and Hippocampal Dentate/CA3 Underlies Age-Related Object Pattern Separation Deficits. Neuron. 2018;97:1187–98.e4. [DOI] [PubMed] [PMC]
72. Dickson DW, Crystal HA, Bevona C, Honer W, Vincent I, Davies P. Correlations of synaptic and pathological markers with cognition of the elderly. Neurobiol Aging. 1995;16:285–98. [DOI] [PubMed]
73. Schmitz C, Rutten BPF, Pielen A, Schäfer S, Wirths O, Tremp G, et al. Hippocampal neuron loss exceeds amyloid plaque load in a transgenic mouse model of Alzheimer's disease. Am J Pathol. 2004;164: 1495–502. [DOI] [PubMed] [PMC]
74. Liu F, Sun J, Wang X, Jin S, Sun F, Wang T, et al. Focal-type, but not Diffuse-type, Amyloid Beta Plaques are Correlated with Alzheimer's Neuropathology, Cognitive Dysfunction, and Neuroinflammation in the Human Hippocampus. Neurosci Bull. 2022;38:1125–38. [DOI] [PubMed] [PMC]
75. Stevens DA, Workman CI, Kuwabara H, Butters MA, Savonenko A, Nassery N, et al. Regional amyloid correlates of cognitive performance in ageing and mild cognitive impairment. Brain Commun. 2022;4: fcac016. [DOI] [PubMed] [PMC]
76. Kawarabayashi T, Younkin LH, Saido TC, Shoji M, Ashe KH, Younkin SG. Age-dependent changes in brain, CSF, and plasma amyloid (beta) protein in the Tg2576 transgenic mouse model of Alzheimer's disease. J Neurosci. 2001;21:372–81. [DOI] [PubMed] [PMC]
77. Tu S, Okamoto S, Lipton SA, Xu H. Oligomeric Aβ-induced synaptic dysfunction in Alzheimer's disease. Mol Neurodegener. 2014;9:48. [DOI] [PubMed] [PMC]
78. Zhang H, Jiang X, Ma L, Wei W, Li Z, Chang S, et al. Role of Aβ in Alzheimer's-related synaptic dysfunction. Front Cell Dev Biol. 2022;10:964075. [DOI] [PubMed] [PMC]
79. Ripoli C, Cocco S, Puma DDL, Piacentini R, Mastrodonato A, Scala F, et al. Intracellular accumulation of amyloid-β (Aβ) protein plays a major role in Aβ-induced alterations of glutamatergic synaptic transmission and plasticity. J Neurosci. 2014;34:12893–903. [DOI] [PubMed] [PMC]

80. Shankar GM, Li S, Mehta TH, Garcia-Munoz A, Shepardson NE, Smith I, et al. Amyloid-beta protein dimers isolated directly from Alzheimer's brains impair synaptic plasticity and memory. Nat Med. 2008;14:837–42. [DOI] [PubMed] [PMC]
81. Jürgensen S, Ferreira ST. Nicotinic receptors, amyloid-beta, and synaptic failure in Alzheimer's disease. J Mol Neurosci. 2010;40:221–9. [DOI] [PubMed]
82. Roberts JP, Stokoe SA, Sathler MF, Nichols RA, Kim S. Selective coactivation of α7- and α4β2-nicotinic acetylcholine receptors reverses beta-amyloid-induced synaptic dysfunction. J Biol Chem. 2021;296: 100402. [DOI] [PubMed] [PMC]
83. Walsh DM, Klyubin I, Fadeeva JV, Rowan MJ, Selkoe DJ. Amyloid-beta oligomers: their production, toxicity and therapeutic inhibition. Biochem Soc Trans. 2002;30:552–7. [DOI] [PubMed]
84. Billings LM, Oddo S, Green KN, McGaugh JL, LaFerla FM. Intraneuronal Abeta causes the onset of early Alzheimer's disease-related cognitive deficits in transgenic mice. Neuron. 2005;45:675–88. [DOI] [PubMed]
85. McLean CA, Cherny RA, Fraser FW, Fuller SJ, Smith MJ, Beyreuther K, et al. Soluble pool of Abeta amyloid as a determinant of severity of neurodegeneration in Alzheimer's disease. Ann Neurol. 1999; 46:860–6. [DOI] [PubMed]
86. Esparza TJ, Zhao H, Cirrito JR, Cairns NJ, Bateman RJ, Holtzman DM, et al. Amyloid-β oligomerization in Alzheimer dementia versus high-pathology controls. Ann Neurol. 2013;73:104–19. [DOI] [PubMed] [PMC]
87. Esparza TJ, Wildburger NC, Jiang H, Gangolli M, Cairns NJ, Bateman RJ, et al. Soluble Amyloid-beta Aggregates from Human Alzheimer's Disease Brains. Sci Rep. 2016;6:38187. [DOI] [PubMed] [PMC]
88. Richetin K, Leclerc C, Toni N, Gallopin T, Pech S, Roybon L, et al. Genetic manipulation of adult-born hippocampal neurons rescues memory in a mouse model of Alzheimer's disease. Brain. 2015;138: 440–55. [DOI] [PubMed]
89. Krezymon A, Richetin K, Halley H, Roybon L, Lassalle J, Francès B, et al. Modifications of hippocampal circuits and early disruption of adult neurogenesis in the tg2576 mouse model of Alzheimer's disease. PLoS One. 2013;8:e76497. [DOI] [PubMed] [PMC]
90. Piatti VC, Ewell LA, Leutgeb JK. Neurogenesis in the dentate gyrus: carrying the message or dictating the tone. Front Neurosci. 2013;7:50. [DOI] [PubMed] [PMC]
91. McHugh SB, Lopes-Dos-Santos V, Gava GP, Hartwich K, Tam SKE, Bannerman DM, et al. Adult-born dentate granule cells promote hippocampal population sparsity. Nat Neurosci. 2022;25:1481–91. [DOI] [PubMed] [PMC]
92. Bardaweel SK, Alzweiri M, Ishaqat AA. D-Serine in neurobiology: CNS neurotransmission and neuromodulation. Can J Neurol Sci. 2014;41:164–76. [DOI] [PubMed]